Reflectance spectroscopy applied to mapping the hydrothermal alteration at the Mamão gold deposit, Andorinhas Greenstone Belt, Carajás Mineral Province, Northern Brazil

Sebastião Rodrigo Cortez de Souza[1]* [ID], Diego Fernando Ducart[2] [ID], Nilson Francisquini Botelho[3] [ID]

Abstract

The Mamão gold deposit is located in the eastern portion of the Amazonian Craton, Northern Brazil, and hosted in Archean metamafic rocks of the Andorinhas greenstone belt. Troy Resources Ltd. mined the deposit between 2008 and 2015, producing about 350 koz via underground operation. The deposit exhibits structural and mineralogical characteristics that allow its classification as an orogenic gold deposit. Reflectance spectroscopy is a non-destructive, fast, and low-cost technique that was applied in drill cores at the Mamão deposit to map and refine stages of hydrothermal alteration. The hydrothermal alteration is marked by a distal or chlorite zone; an intermediate or carbonate zone; a proximal or potassic zone, and a gold-rich quartz vein-hosted orebody. The reflectance spectroscopy has confirmed the diversified mineralogical compositions (tourmaline, amphibole, mica, epidote, carbonate, and chlorite) observed along the hydrothermal zones, having been confirmed by a petrographic study. The study has also demonstrated that chlorite abundance decreases from the edge to the center of the altered profile, proving a fast and reliable result to the mapping of the hydrothermal halos in Archean greenstone belts, which is an important tool for the vectoring of gold mineralization, acting as an excellent mineral prospecting tool.

KEYWORDS: Archean gold deposit; reflectance spectroscopy; mineral mapping; hydrothermal alteration; Amazonian craton.

INTRODUCTION

Several gold deposits are related to Archean granite-greenstone terrains worldwide (Goldfarb *et al.* 2001, Groves *et al.* 2016, Nguimatsia *et al.* 2017). Mining activity in the Rio Maria region (Pará state, Brazil) has been traditionally linked to gold mineralization since the 1970s, where the gold has been extracted from the alluvial artisanal or small-scale mining or "garimpos." Some orogenic-type gold deposits (such as Mamão, Lagoa Seca, Coruja, and Babaçu) are located in this sequence, named Andorinhas greenstone belt (Costa e Silva *et al.* 2012, Souza *et al.* 2020, Souza *et al.* 2021).

The Mamão gold deposit is a mechanized underground mining, located about 40 km southeast of Rio Maria city. This deposit is located in the Rio Maria Domain, in the southeast portion of Carajás Mineral Province (CMP). It was operated between 2008 and 2015 by Reinarda Mineração Ltda.

[1]Universidade Federal de Pernambuco, Departamento de Geologia – Recife (PE), Brazil. E-mail: rodrigo.cortez@ufpe.br

[2]Universidade Estadual de Campinas, Instituto de Geociências, Campinas (SP), Brazil. E-mail: dducart@unicamp.br

[3]Universidade de Brasília, Instituto de Geociências, Brasília (DF), Brazil. E-mail: nilsonfb@unb.br

*Corresponding author.

company (a Troy Resources subsidiary), having extracted an amount of approximately 350 koz gold with head grades around 6 g/t Au, locally reaching more than 100 g/t Au due to the nugget effect (Souza *et al.* 2021).

Mineralization is related to quartz-carbonate-sulfide lodes of high-grade/free gold mineralization within sheared-hosted metabasalts and metadolerites of the Archean age (Souza *et al.* 2021). Mineralization occurs on a structural trend, on ENE-WSW shear zones with better development of orebodies at EW trending bends, filling out dilational jogs on a high-strain zone within the metavolcanic rocks of Andorinhas greenstone bel (Costa e Silva *et al.* 2012, Souza *et al.* 2021).

Reflectance spectroscopy is a method that has been progressively utilized in mineral exploration. It is a widely known technique for pointing out the minerals within altered hydrothermal zones of the mineral deposits, especially useful for field and active exploration work. This technique is non-destructive and simple to use, and it can quickly provide large quantities of data (Herrmann *et al.* 2001, Harraden *et al.* 2013). The technique is based on the interaction of electromagnetic energy at 350–2500 nm wavelengths and the surface of materials (Clark 1999). Specifically, the energy at the 1300–2500 nm wavelength range (short-wave infrared (SWIR) region) interacts, through vibrational processes with molecular bonds in H_2O, NH^4, SO^4, and CO_3^{2-} and with cation ^-OH bonds in Al–OH, Mg–OH, and Fe–OH (Clark 1999, Hunt 1977). As a result of this interaction, different absorption features are produced in specific wavelengths.

The use of reflectance spectroscopy is routinely applied in the study of the Phanerozoic slightly or non-deformed porphyry-, epithermal-, IOCG-, and VMS-type gold deposits (Herrmann *et al.* 2001, Squire *et al.* 2007, Tappert *et al.* 2011, Mauger *et al.* 2016, among others). However, less research has been performed on pre-Phanerozoic deformed orogenic gold deposits (Travers and Wilson 2015, Wilson *et al.* 2009, Arne *et al.* 2016, Sandeman *et al.* 2010). Thompson *et al.* (1999) suggested that different hydrothermal alteration zones might be mapped using reflectance spectroscopy techniques and used for mineral exploration applications on Archean orogenic gold deposits. Recently, Naleto *et al.* (2019) studied the Paleoproterozoic orogenic Pedra Branca gold deposit (Tróia Massif, Borborema Province, Northeast Brazil) using spectroscopic data to investigate and characterize the hydrothermal paragenesis, with the aim of developing mineral exploration guides in the region.

The use of a reflectance spectroscopy analysis allows elucidation of the history of hydrothermal systems related to these gold deposits, providing parameters that, when integrated with petrographic studies, are capable of showing the evolution of the mineralizing process, the spatial location, and the distribution of the ore. Hydrothermal alterations form variable dimensions zones that relate directly to the style of mineralization, metal ratios, and physical-chemical rock properties with implications for genetic and resource modeling of the deposit (Gregory *et al.* 2013). Alteration mineral assemblages are important to the understanding of the hydrothermal process where ore deposits were formed. Determination of the type and distribution of alteration minerals is a routine part of mineral exploration and is useful in the assessment of exploration properties and the construction of deposit models.

This paper evaluates the application of reflectance spectroscopy for the study of hydrothermal alteration in the Mamão gold deposit, which can help to link hydrothermal alteration types with the concentration of economic gold content and illustrate potential contributions of the method to the understanding of the hydrothermal evolution of the orogenic gold deposit.

GEOLOGICAL SETTING

Regional geology

The CMP is the largest and best-preserved Archean segment of the Amazonian craton (Fig. 1a), in northern Brazil (Dall'Agnol *et al.* 2006, Vasquez *et al.* 2008). It was formed in the Mesoarchean and tectonically stabilized in the Neoarchean (Tassinari and Macambira 1999, 2004). It represents one of the most important mineral provinces in the world, standing out for its diversity and notable metallogenetic potential, including a broad range of deposits such as iron (e.g., N4 and N5), iron-oxide–copper–gold (e.g., Salobo and Sossego), manganese
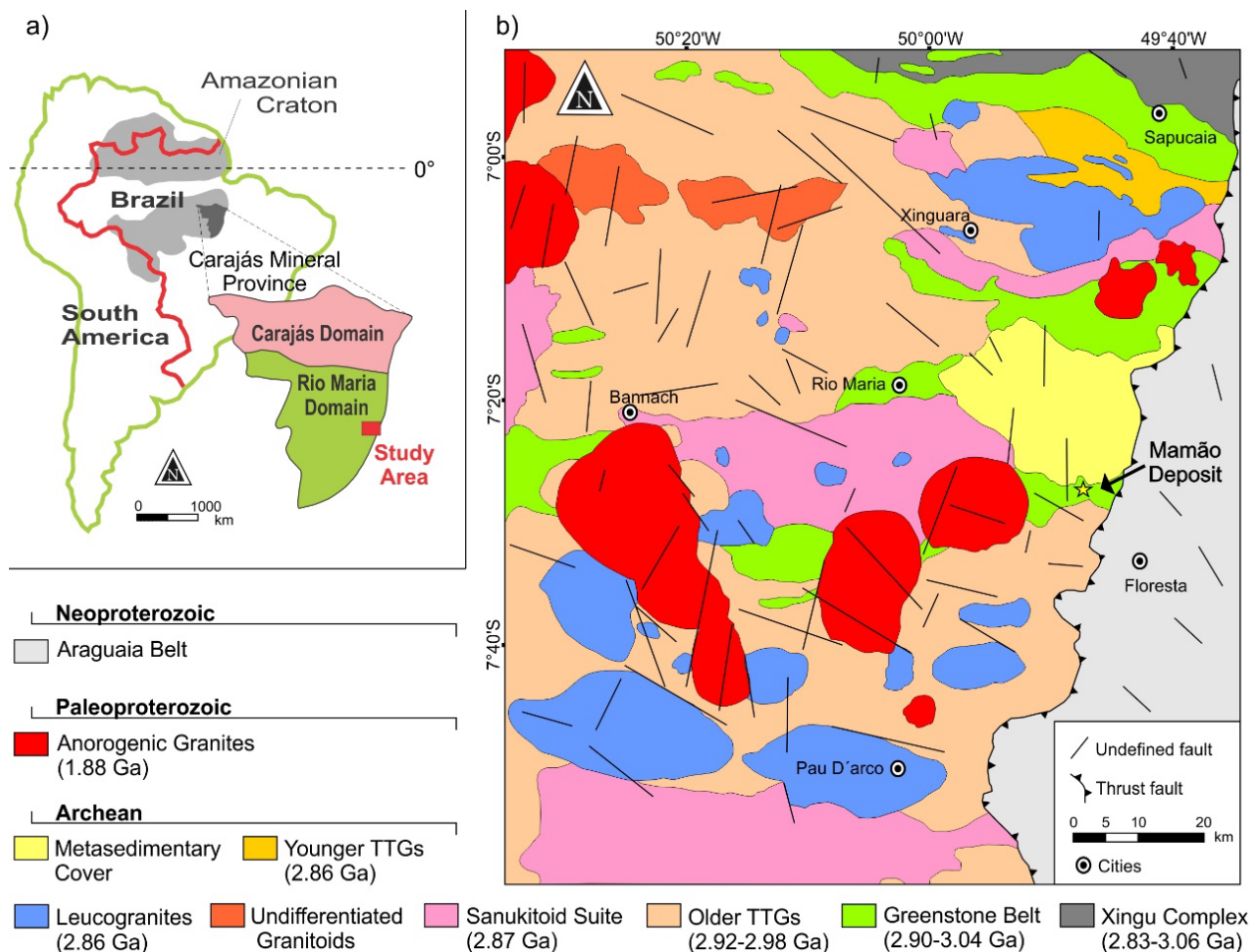

Figure 1. (a) Simplified map of the Amazonian Craton, showing the Carajás Mineral Province and the study area location highlighted. (b) Geological map of the Rio Maria domains and location of the studied area in Amazonian Craton (modified after Almeida *et al.* 2013).

(e.g., Azul, Buritirama), nickel (e.g., Vermelho and Onça-Puma), chrome-PGE (e.g., Luanga), gold–palladium–platinum (e.g., Serra Pelada), and copper–molybdenum–gold deposits (e.g., Serra Verde; Dardenne and Schobbenhaus 2001, Villas and Santos 2001). It is considered one of the most important mineral provinces of fertile metallogenetic exploration (Dardenne and Schobbenhaus 2001, Villas and Santos 2001, Bettencourt *et al.* 2016). CMP is divided into two distinct tectonic domains: Rio Maria Domain (Mesoarchean) at the south, with a predominance of granite-greenstone terrains (ages ranging from 2.85 to 3.04 Ga), and Carajás Domain (Neoarchean) to the north, characterized by metavolcano-sedimentary and granitoid sequences generated mainly between 2.76 and 2.55 Ga (Fig. 1a) (Vasquez *et al.* 2008).

The Xingu Complex is interpreted as the basement of the CMP (~2.83–3.06 Ga), composed of high-grade orthogneiss (Vasquez *et al.* 2008). The Mamão deposit, which is located in the Rio Maria Domain, is hosted by Archean supracrustal greenstone belt sequences and granitoids (Fig. 1b). The greenstone belt sequences are grouped on Andorinhas Supergroup and represent the oldest lithostratigraphic unit of the region. These rocks display different grades of deformation and greenschist facies metamorphism, which are composed of ultramafic and mafic metavolcanic rocks intercalated with iron formations and intermediate to felsic rocks at the base (Babaçu Group) and clastic metasedimentary rocks at the top (Lagoa Seca Group) (Souza *et al.* 2001). The metavolcanic rocks host small lode gold deposits (*e.g.,* Mamão, Babaçu, and Coruja), while other deposits are associated with the metagreywacke (Lagoa Seca) (Huhn 1992, Souza 1999, Souza 2018) (Fig. 2).

Archean granitoids intrude the greenstone belt sequence and can be assembled in four groups:
- an older TTG series composed of Arco Verde tonalite complex (2.98–2.92 Ga) (Althoff *et al.* 2000);
- a sanukitoid suite represented by the Rio Maria granodiorite (~2.87 Ga; Oliveira *et al.* 2009);
- a younger TTG series (~2.87–2.86 Ga), represented by the Mogno trondhjemite (Almeida *et al.* 2011, Almeida *et al.* 2013);
- potassic leucogranites of calc-alkaline affinity (~2.87–2.86 Ga) represented by the Xinguara granite pluton (Leite *et al.* 2004).

Paleoproterozoic anorogenic alkaline to subalkaline A-type granitoid stocks and batholiths cut the greenstone belt rocks (Dall'Agnol *et al.* 2006). The Araguaia Belt is composed of a metamorphosed psammitic and pelitic sequence with minor contributions of chemical sediments and mafic and ultramafic rocks (Vasquez *et al.* 2008) (Fig. 1b).

Local geology

The geology of the study area was first described by DOCEGEO (1988). It classified the rocks in the Babaçu Group, which comprises tholeitic metabasalt flow, accompanied by pillow lava structures and intensive intercalations of banded iron formations, metatuffs, metaultramafic (talc-chlorite-schists), metachert, and subordinate metadacites rocks, which are intruded by dolerite dikes. Metabasalt to mafic schist are fine-grained rocks, sometimes magnetic, deformed, and metamorphosed at greenschist facies. Recently, the Geological
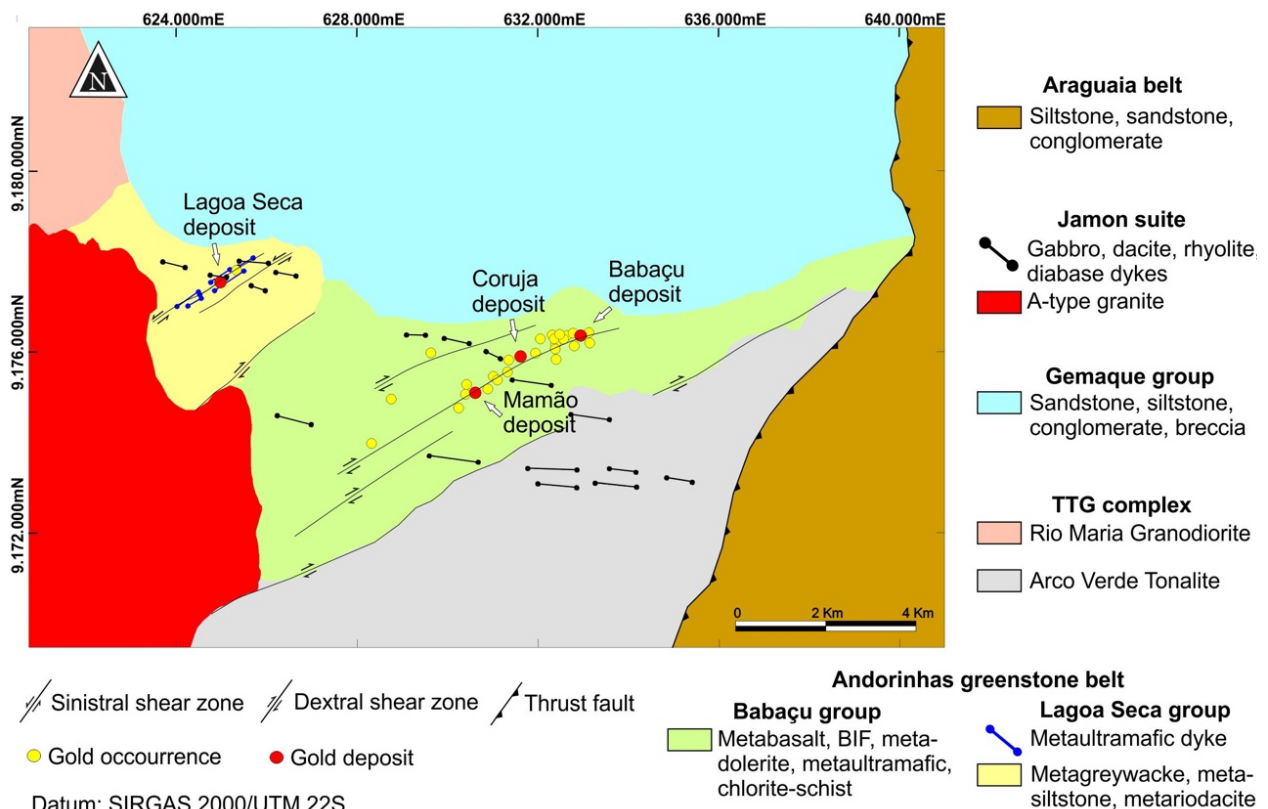

Datum: SIRGAS 2000/UTM 22S

Source: Souza (2018).

Figure 2. Geological map of the Andorinhas greenstone belt.

Survey of Brazil (CPRM) carried out a basic geological mapping program comprising the study area (Sabóia *et al.* 2018). In this study, the Babaçu Group has been renamed to the Andorinhas Group, consisting of the Babaçu Formation at the base and the Lagoa Seca Formation at the top, which does not outcrop in the study area. Gold occurrences are associated with quartz veins and/or quartz-carbonate veinlets, followed by strong hydrothermal alteration. Figure 2 shows the geological mapping carried out by Troy Resources Ltd. and summarized by Souza (2018).

Gold mineralization

The Mamão gold deposit comprises two tabular orebodies, called Melechete and M2, both mineralized for 500 m along strike and at least 600 m down dip (Souza *et al.* 2021). The gold deposits occur in structurally controlled quartz veins within the metabasalts and metadolerites greenstone belt rocks (Fig. 3a). The oreshoots have an NE plunge along ENE-WSW trending shear zones dipping 30–60° to the north (Fig. 3a). These shear zones started as surfaces of reverse movement and were reactivated in a later stage as surfaces of normal displacement. Gold was introduced by sulfide-rich fluids that percolated these shear zones, and the mineralization style at Mamão deposit is classified as gold-rich orogenic-type (Souza *et al.* 2021) or shear-zone related lode-gold (Villas and Santos 2001), in contrast to IOCG-type deposits at Carajás Domain that are characteristically base metal poor-gold deposits (Melo *et al.* 2017, Craveiro *et al.* 2019, Melo *et al.* 2019).

The mineralized zones are composed of quartz veins and veinlets in a shear zone that cuts quartz-carbonate-chlorite schist, which sometimes shows a strong mylonitic foliation marked by the preferential orientation of chlorite and biotite lamellae and by quartz-carbonate-rich and chlorite-mica-rich bands on altered metavolcanic host rocks (Souza 2018).

Quartz veins were formed during the alteration process and are oriented parallel or subparallel to the mylonitic foliation. Their thickness varies from 0.5 to 5 m with an average thickness of around 2 m (Fig. 3a). The higher grades of mineralization are associated with massive silica replacement and quartz veins (Figs. 3b and 3c).
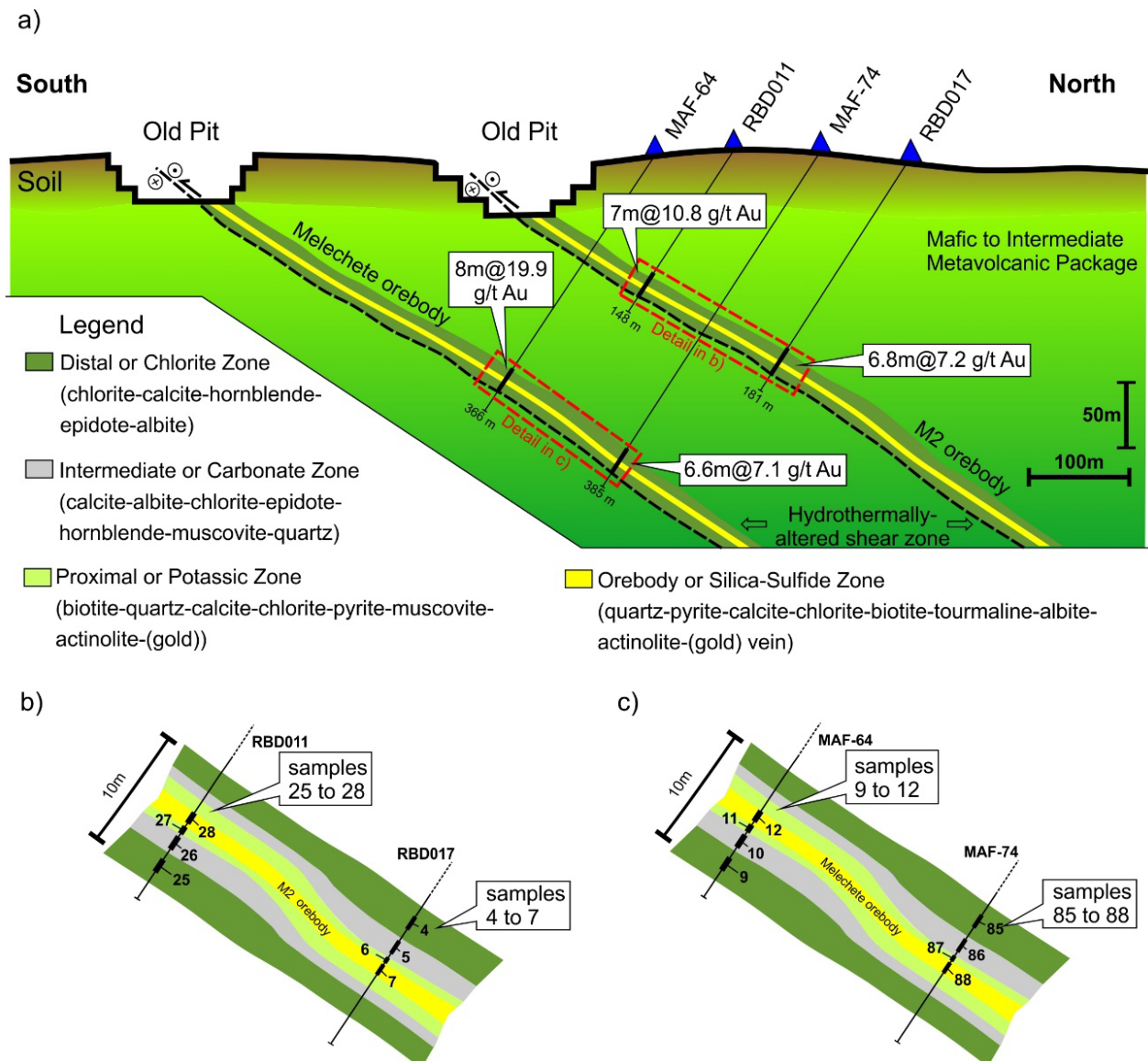

Figure 3. (a) Schematic cross section showing the mineralization in the Mamão deposit, according to Souza (2018). (b) Detail of the M2 orebody and its hydrothermal alteration zoning. (c) Detail of the Melechete orebody and its hydrothermal alteration zoning.

Hydrothermal alteration zones

The paragenetic sequence of the hydrothermal minerals of the Mamão deposit can be observed in Figs. 3b, 3c, and 4 (Souza *et al.* 2021, after Tunussi 2012). It is composed of pyrite, biotite, quartz, carbonate, biotite, muscovite, chlorite, and gold, occurring as replacement products of the original mineral assemblages. This assemblage indicates at least four hydrothermal alteration zones, including chlorite-calcite-hornblende-epidote-albite (distal or chlorite zone), calcite-albite-chlorite-epidote-hornblende-muscovite-quartz (intermediate or carbonate zone), biotite-quartz-calcite-chlorite-pyrite-muscovite-actinolite-(gold) (proximal or potassic zone), and quartz-pyrite-calcite-chlorite-biotite-tourmaline-albite-actinolite-(gold) (orebody or silica-sulfide zone) (Fig. 5).

The hydrothermal alteration reaches up to a width of 10 m. The outermost part of alteration comprises the distal and intermediate zones, which are characterized by chlorite and carbonate alteration, respectively, varying from 3 to 5 m in width. The inner altered zone is filled by proximal and ore zones, which are marked by pervasive potassic alteration (biotite) and strong silicification and sulfidation process plus gold deposition, culminating in the quartz vein formation. The inner mineralized package presents a width of 1–5 m.

MATERIALS AND METHODS

A total of 16 geological samples were obtained at four diamond drill cores that cut hydrothermal and ore zones of the Mamão deposit. From these samples, specifically, eight samples correspond to two drill holes of the Melechete orebody (MAF-64 and MAF-74) and another eight samples to two drill holes of the M2 orebody (RBD011 and RBD017, as the core samples from drill holes MAF-64 and MAF-74 were incomplete). Petrographic studies were performed on thin/polished sections using the Olympus Microscope Model BX60FS (Olympus Optical Co. Ltd.) from the Microscopy Laboratory of the Universidade de Brasília.

A reflectance study was obtained using an Analytical Spectral Devices (ASD)/FieldSpec-3 Hi-Res® spectroradiometer directly on selected diamond drill core intervals. The measurements were carried out using a contact probe coupled to a halogen lamp as the luminous source. The window

acquisition comprises an area of 1 cm², and the final spectrum is the average of about 70 spectra obtained in the process. The spectra are collected in three stages, covering the wavelengths of visible to near-infrared (VNIR: 350–1,000 nm) to the SWIR (1,000–2,500 nm). The spectral resolution is 3 nm (VNIR) and 6 nm (SWIR) to the analytical records, with sampling intervals of 1.4 nm (VNIR) and 1.1 nm (SWIR). The spectra collected by the spectroradiometer were converted from radiation to reflectance using a Spectralon™ panel, collected through a calibration made every 20 min during the data collection.

A total of 47 spectra were measured in the laboratory and duly photographed for sample orientation and results location. Spectral data were processed, analyzed, and interpreted through "The Spectral Geologist" (TSG-8) commercial software and following established spectroscopy works of Hunt and Salisbury (1970, 1971), Hunt and Ashley (1979), Clark (1999), and Bishop *et al.* (2008). Specific absorption features were also analyzed to investigate the abundance and chemical composition of chlorites and carbonates. The composition of chlorite is based on the wavelength of the Mg–OH absorption feature at ~2,350 nm (McLeod *et al.* 1987). The wavelength of this absorption feature increases as the iron content of chlorite increases. Wavelengths of Mg–OH absorption between 2,331 and 2,337 nm are related to Mg-rich chlorite, between 2,337 and 2,347 nm to Fe-Mg chlorite, and between 2,347 and 2,358 nm to Fe-rich chlorite. The abundance of chlorite was defined considering the depth of the Mg–OH absorption at ~2,350 nm. The composition of carbonate is based on the wavelength of CO_3^{2-} absorption feature at ~2,340 nm (Hunt and Salisbury 1971). The wavelength of CO_3^{2-} absorption is between 2,340 and 2,345 for calcite.

The values and curves of linear correlation (R^2) for chlorite abundance were obtained using *Microsoft Excel*® spreadsheets.

RESULTS

The reflectance spectroscopy results obtained in drill cores of the Melechete and M2 orebodies are shown in Figs. 6 and 7. The figures also note the sampling position in relation to the equivalent hydrothermal alteration zones. The diamond drill holes related to the Melechete orebody are represented by MAF-64 (samples 9–12) and MAF-74 (samples 85–88). The drill holes related to the M2 orebody are represented by RBD011 (samples 25–28) and RBD017 (samples 4–7).

The spectral data extracted by reflectance spectroscopy for the Melechete orebody can be observed in Fig. 6, obtained through each hydrothermal alteration zone. The analysis of samples 9 and 85 indicated the presence of calcite and FeMg chlorites. Samples 10 and 86 returned FeMg chlorite, sometimes mixed with calcite and hornblende, and a very fine-grained aggregate composed of hornblende-calcite-muscovite. Samples 11 and 87 showed greater mineralogical variability, ranging from calcite, FeMg chlorites, and actinolite up to a mixture of muscovite and biotite micas. Samples 12 and 88 were characterized as calcite, FeMg chlorites, and actinolite. The wavelengths of Mg-OH absorptions for chlorite
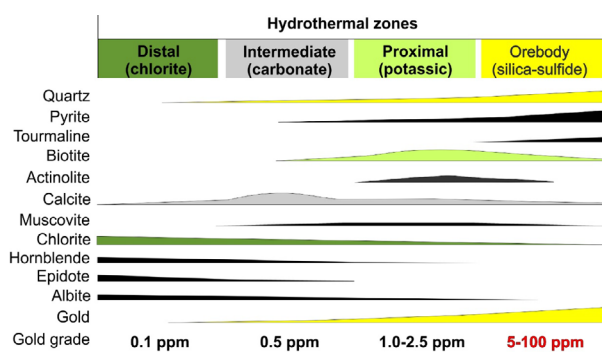
Source: Modified from Souza *et al.* (2021).

**Figure 4.** Paragenetic sequence of hydrothermal alteration in the Mamão deposit.
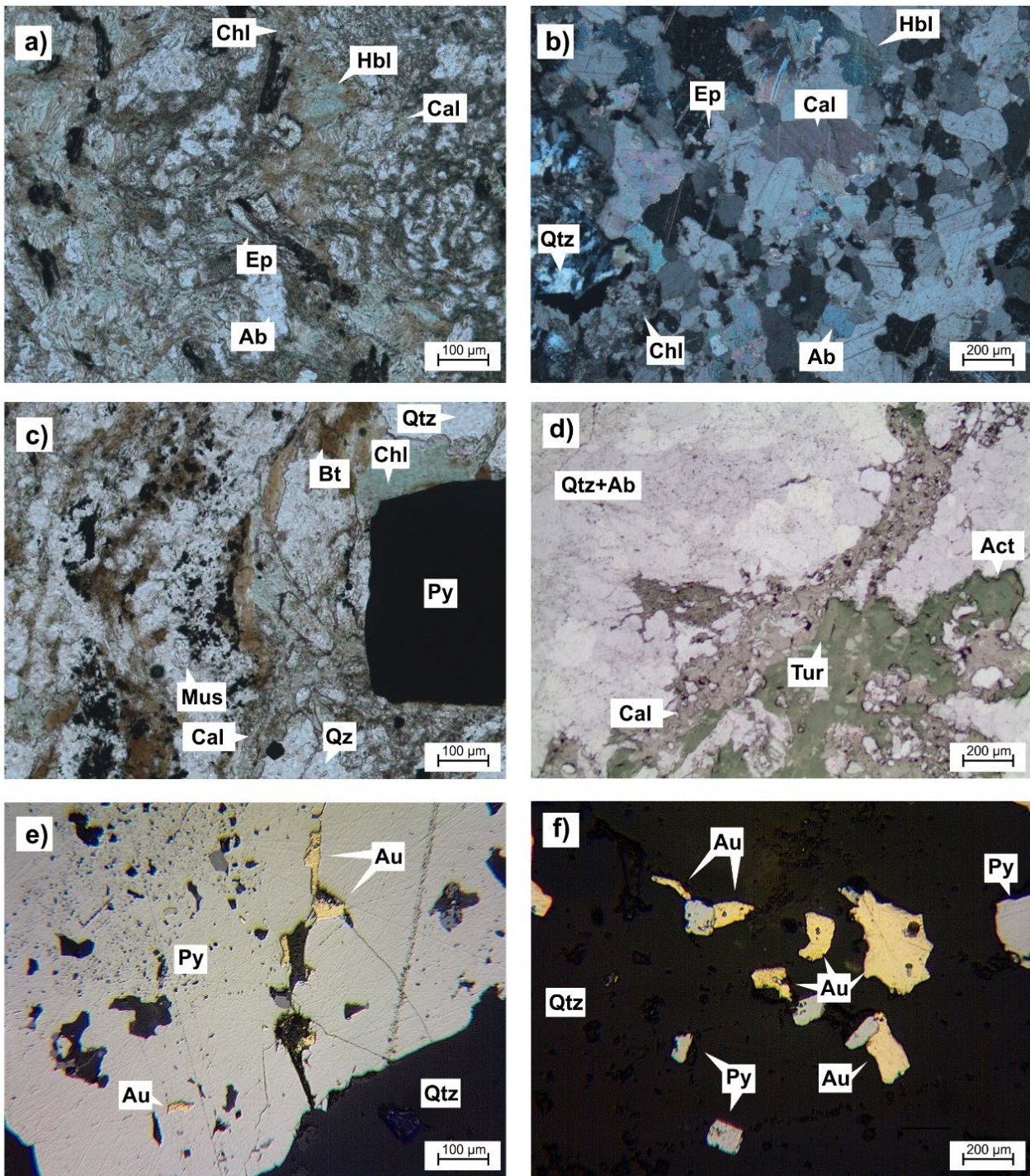
Ab: albite; Act: actinolite; Au: gold; Bt: biotite; Cal: calcite; Chl: chlorite; Ep: epidote; Hbl: hornblende; Mus: muscovite; Qz: quartz; Py: pyrite; Tur: tourmaline; TS: thin section; PS: polished section; PPL: plane-polarized light; XPL: cross-polarized light.

Figure 5. Photomicrographs of hydrothermal alteration and ore assemblages in the Mamão deposit. (a) Distal zone composed of chlorite-calcite-hornblende-epidote-albite (Sample 9 – TS/PPL). (b) Intermediate zone marked by calcite-albite-chlorite-quartz-epidote (Sample 26 – TS/XPL). (c) Proximal zone composed of biotite-quartz-calcite-pyrite-chlorite-muscovite (sample 6 – TS/PPL). (d) Typical quartz vein (orebody zone) characterized by quartz-calcite-albite-tourmaline (Sample 12 – TS/PPL). (e and f) Different gold textures and sizes, occurring as filling fractures (e) or enclosed in pyrite or as well as free particles (f) in the quartz matrix (Sample 28 – PS/PPL).

vary between 2,338 and 2,347 nm, and the CO_3^{2-} absorption wavelengths of carbonates range between 2,332 and 2,339 nm (Table 1).

For the M2 orebody, the spectral data were, at large, very similar to those obtained in the Melechete body (Figure 7). Samples 4 and 25 returned the presence of calcite, FeMg chlorites, and hornblende. Samples 5 and 26 identified the same previous mineralogy, in addition to epidote. Despite showing unusual spectral curves, samples 6 and 27 were classified as calcite and FeMg chlorites. However, in samples 7 and 28, in addition to the presence of calcite and FeMg chlorite, the reflectance also indicated the presence of biotite and tourmaline. The wavelengths of Mg–OH absorptions for chlorite vary between 2,339 and 2,347 nm, and the CO_3^{2-} absorption wavelengths of carbonates range between 2,337 and 2,340 nm (Table 2).
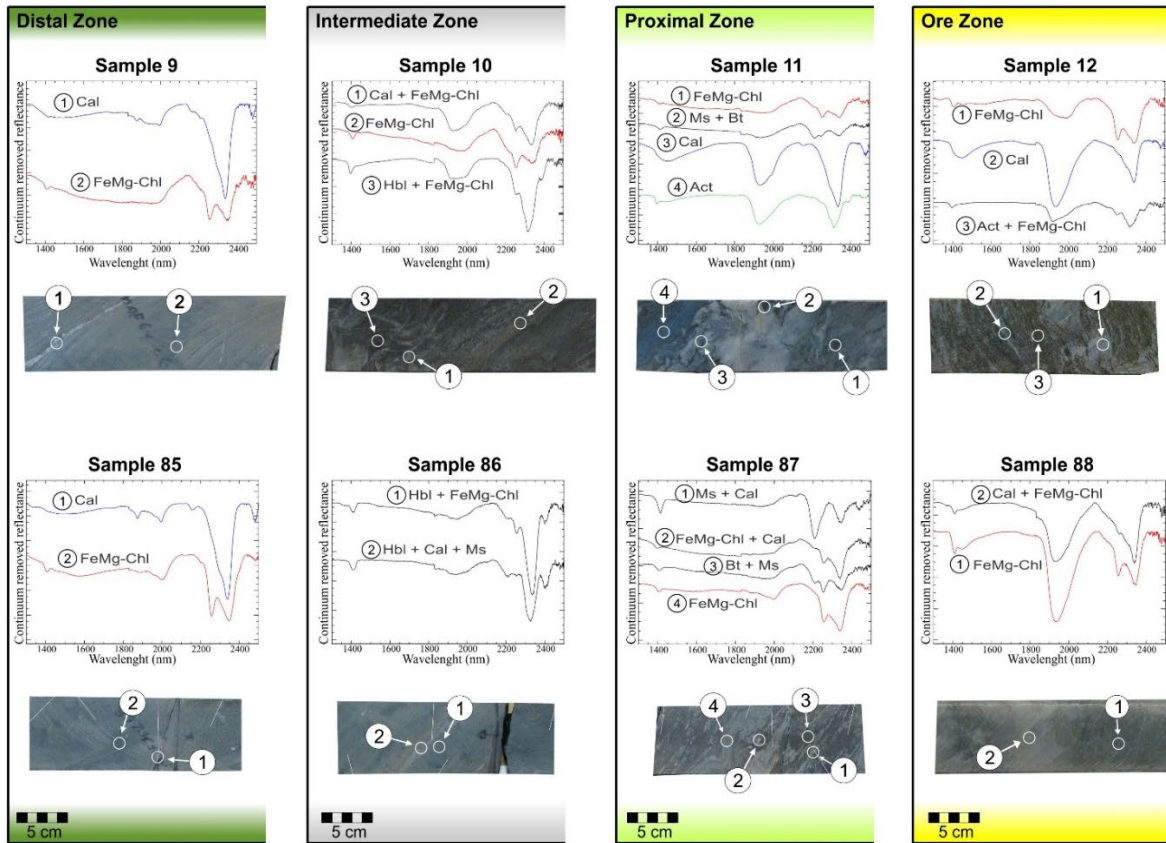
FeMg-Chl: Fe-Mg-chlorite; Cal: calcite; Hbl: hornblende; Act: actinolite; Bt: biotite; Ms: muscovite.
Figure 6. Mineralogy obtained by reflectance spectroscopy on diamond drill cores of the Melechete orebody from the Mamão deposit, classified according to its hydrothermal zone. Spectra are stacked. Rounded absorption features at approximately 1,900 nm are related to water inclusions in quartz. Y-axes of spectra represent continuum-removed reflectance.
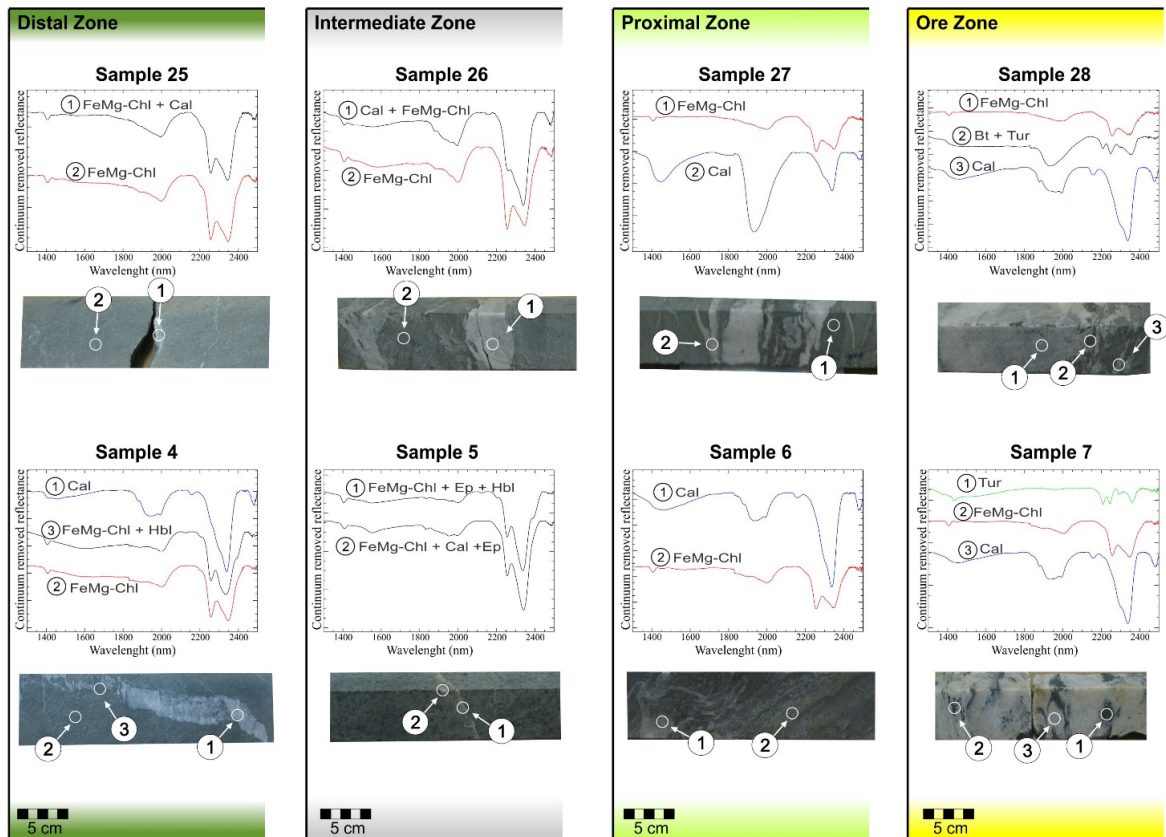
FeMg-Chl: Fe-Mg-chlorite; Cal: calcite; Tur: tourmaline; Bt: biotite; Ep: epidote; Hbl: hornblende.
Figure 7. Mineralogy obtained by reflectance spectroscopy on diamond drill cores of the M2 orebody from the Mamão deposit, classified according to its hydrothermal zone. Spectra are stacked. Y-axes of spectra represent continuum-removed reflectance. Absorption features at approximately 1,900 nm are related to water inclusions in quartz.

Table 1. Representative minerals appointed by reflectance spectroscopy study in the Melechete orebody from the Mamão deposit. Abundance values are relative, in a 0–1 interval (0 = absence). Wavelengths are in nanometer units.

Drill Hole	Sample	Hydrothermal Zone	Detected Minerals	Chlorite		Carbonate
				Abundance	Wavelength	Wavelength
MAF-64	9	Distal	FeMg-Chl, Cal	0.085	2,347	2,339
	10	Intermediate	FeMg-Chl, Cal, Hbl	0.054	2,339	2,338
	11	Proximal	FeMg-Chl, Cal, Act, Bt, Ms	0.067	2,344	2,333
	12	Ore	FeMg-Chl, Cal, Act	0.066	2,338	2,332
MAF-74	85	Distal	FeMg-Chl, Cal	0.209	2,345	2,339
	86	Intermediate	FeMg-Chl, Cal, Hbl, Ms	0.143	2,347	2,332
	87	Proximal	FeMg-Chl, Cal, Bt, Ms	0.095	2,342	2,341
	88	Ore	FeMg-Chl, Cal	0.078	2,343	2,341

FeMg-Chl: Fe-Mg-chlorite; Cal: calcite; Hbl: hornblende; Act: actinolite; Bt: biotite; Ms: muscovite.

Table 2. Representative minerals appointed by reflectance spectroscopy study in the M2 orebody from the Mamão deposit. Abundance values are relative, in a 0–1 interval (0 = absence). Wavelengths are in nanometer units.

Drill Hole	Sample	Hydrothermal Zone	Detected Minerals	Chlorite		Carbonate
				Abundance	Wavelength	Wavelength
RBD011	25	Distal	FeMg-Chl, Cal	0.168	2,346	2,339
	26	Intermediate	FeMg-Chl, Cal	0.153	2,346	2,340
	27	Proximal	FeMg-Chl, Cal	0.132	2,347	2,338
	28	Ore	FeMg-Chl, Cal, Bt, Tur	0.076	2,351	2,340
RBD017	4	Distal	FeMg-Chl, Cal, Hbl	0.185	2,343	2,340
	5	Intermediate	FeMg-Chl, Cal, Ep, Hbl	0.135	2,342	2,337
	6	Proximal	FeMg-Chl, Cal	0.112	2,347	2,339
	7	Ore	FeMg-Chl, Cal, Tur	0.085	2,339	2,337

FeMg-Chl: Fe-Mg-chlorite; Cal: calcite; Tur: tourmaline; Bt: biotite; Ep: epidote; Hbl: hornblende.

DISCUSSION

A robust metallogenetic characterization of the Mamão deposit was recently studied by Souza *et al.* (2021) and the references therein, who concluded that the deposit belongs to the class of orogenic gold deposits, associated with the development of pervasive (proximal) to weak (distal) hydrothermal alteration halos, auriferous quartz lode-centered.

The petrographic study carried out in this study corroborates this statement above, reporting a mineral paragenesis compatible with orogenic type deposits, formed by four different zones, as follows:

i. a distal zone composed of chlorite-calcite-hornblende-epidote-albite;

ii. an intermediate zone, which is marked by calcite-albite-chlorite-albite-epidote-hornblende-muscovite-quartz;

iii. a proximal zone consisted of biotite-quartz-calcite-chlorite-pyrite-muscovite-actinolite-(gold);

iv. a quartz vein-hosted ore zone showing quartz-pyrite-calcite-chlorite-biotite-tourmaline-albite-actinolite-(gold).

The reflectance spectroscopy technique has been applied in the same intervals assayed in the petrographic study, showing a good correlation between the results obtained, as already well demonstrated in the literature. For example, chlorite, calcite, and amphibole are present in all hydrothermal zones, from distal and intermediate zones to the mineralized proximal and ore zones. Epidote is found in the intermediate zone, while mica has been found in the intermediate, proximal, and ore zones. Tourmaline occurs in the ore zone. The technique has limitations in identifying quartz and gold minerals, due to its very low chemical reactivity, which directly affects the spectral signature of the mineralized zone. However, the spectral signatures in the zones around the ore were successfully obtained, and lend themselves perfectly as mineralization guides.

Analyzing more carefully, chlorite is Fe-Mg-rich and appears along all alteration zones, which is totally compatible with the geochemistry of the host metamafic rocks of the deposit. Muscovite is in the intermediate do proximal zones, while biotite is typical of internal mineralized intervals (proximal and ore zone) and reflects the potassic alteration developed. Calcite is well-established under all hydrothermal zoning. However, the presence in the ore zone would indicate a basic CO_2-rich fluid, favoring a decrease in both pH and Eh, leading to the deposition of gold in this environment (Gilbert *et al.*, 1998). Amphibole has a hornblende composition in the distal to intermediate zones, which is replaced by actinolite in the proximal to ore zones, and this mineralogical variation reflects the decrease in temperature, which must have been higher in the distal hosted rocks (greenschist to amphibolite

facies temperature) than in the proximal center of the hydrothermal alteration (low greenschist facies temperature).

The chlorite abundance calculated by reflectance spectroscopy analysis shows a tendency, in general terms, to decrease from the edge to the center of the hydrothermal alteration (Fig. 8), ranging from 0.168–0.185 in the edge to 0.076–0.085 in the core alteration of the M2 lode (Table 2) and from about 0.200 in the edge to 0.066–0.078 in the core alteration of the Melechete lode (Table 1). Chlorite abundance curves, which are calculated from the edge to the center, obey a negative linear correlation with more than 90% accuracy ($R^2 = 0.91$, $R^2 = 0.94$, and $R^2 = 0.97$; Fig. 8). These data are fully supported in accordance with previously performed petrography data (Fig. 5). However, in the Melechete orebody, specifically in the distal and intermediate zones (samples 9 and 10, respectively) of the MAF-64 drill hole, the calculated chlorite abundance was abruptly lower than normal, varying between 0.054 and 0.085 (Table 1), performing a linear regression curve with $R^2 = 0.20$. A probable cause for this below-average chlorite abundance can be explained by mineralogical heterogeneity produced by non-pervasive hydrothermal alteration, typical of distal zones, which can lead, locally, to a lower concentration of chlorite.

Thus, all the reflectance spectroscopy data here obtained are totally pertinent to the expected and prove that the reflectance spectroscopy technique can give a fast and reliable result, tracing hydrothermally altered rocks to refine gold mineral exploration. Chlorite is an abundant mineral in the peripheral hydrothermal zones of metamafic-hosted rocks, however, being almost entirely replaced by other alteration styles in the internal part, mainly potassic alteration, silicification, and sulfidation, which are related to the presence of gold mineralization in the deposit.
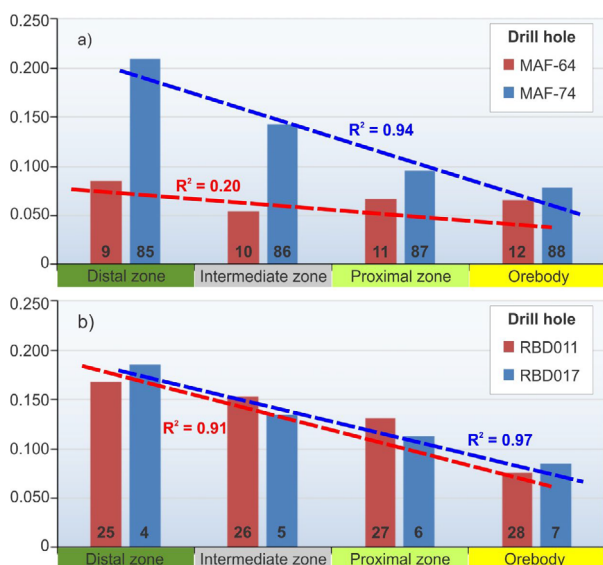
Unfortunately, in this study, it was not possible to determine the abundance of carbonates and micas, as well as other minerals from hydrothermal paragenesis, and thus further refine the RE technique, due to either the limitations of the software used or the low capacity to acquire reliable readings in very small and irregular surfaces. A more in-depth study of mineral chemistry in hydrothermal minerals can also help produce more robust and assertive results.

CONCLUSION

This study used reflectance spectroscopy to characterize the hydrothermal alteration in the Mamão gold deposit, which is an Archean orogenic-style gold deposit located in the Andorinhas greenstone belt, CMP, Brazil. The aim of the research was to identify vectors of gold mineralization in the area through mineral mapping, providing a new tool for the mineral industry operating in similar geological and metallogenetic terrains, widely distributed in Brazilian greenstone belts (Pará, Amapá, Goiás, Minas Gerais, Bahia state, etc.) and other countries (Canada, Australia, Guyana, and Venezuela, among others).

A petrographic study carried out in the Mamão gold deposit divided the hydrothermal alteration into four zones, from the edge to the center, as follows: distal (or chlorite zone), intermediate (or carbonate zone), proximal (or potassic zone), and orebody (or silica-sulfide zone). Using reflectance spectroscopy, despite the few samples analyzed in this study, which was carried out on an experimental basis, the mineralogy obtained was able to confirm the previous petrographic study, even with the operational limitations found in the use of the technique. The hydrothermal evolution could be traced using the spectral analysis and the result confirms the four phases followed by diversified mineralogical dimensions and compositions, culminating with the deposition of gold in the ore zone dominated by quartz-pyrite-calcite-biotite-chlorite-muscovite-actinolite-toumaline-(gold).

Chlorite (Fe-Mg-rich) and carbonate were found in all zones, while hornblende, muscovite, and epidote were described in the outer zones (distal and intermediate) and tourmaline, actinolite, and biotite were described in the inner zones (proximal and orebody). The spectral abundance of the mineral chlorite was estimated and showed that its quantity decreases from the edge to the center of the hydrothermal alteration, in the order of average magnitude of 0.180–0.075, respectively, with linear correlation greater than 90% assertiveness in three of the four simulated situations. Consequently, the spectral behavior reflects exactly the same mineralogical behavior of chlorite, observed in petrography.

This study has shown a positive correlation between reflectance spectroscopy and petrographic techniques. Is possible to carry out a very fast and low-cost characterization survey directly in the drill cores or even in chip/grab samples where hydrothermally altered rocks outcrop. Using spectral mapping of chlorite, we may estimate the decrease in its abundance vectorizing toward internal areas of the hydrothermal package, where there is the greatest possibility of developing proximal alterations (potassic) or even gold-rich quartz veins orebody.

Figure 8. Chlorite abundance (Y-axes of spectra) calculated by reflectance spectroscopy algorithm, arranged according to their corresponding hydrothermal alteration zone. Samples are represented by internal numbers. (a) Chlorites from Melechete orebody. (b) Chlorites from M2 orebody. Internal numbers represent the number of analyzed samples. R^2 represents the linear correlation between the data obtained.

Thus, reflectance spectroscopy becomes an important and robust tool to assist field mapping in mineral exploration at Archean (Paleoproterozoic maybe) greenstone belts.

REFERENCES

Almeida J.A.C., Dall'Agnol R., Leite A.A.S. 2013. Geochemistry and zircon geochronology of the Archean granite suites of the Rio Maria granite-greenstone terrane, Carajás Province, Brazil. *Journal of South American Earth Sciences*, **42**:103-126. https://doi.org/10.1016/j.jsames.2012.10.008

Almeida J.A.C., Dall'Agnol R., Oliveira M.A., Macambira M.J.B., Pimentel M.M., Rämö O.T., Guimarães F.V., Leite A.A.S. 2011. Zircon geochronology, geochemistry and origin of the TTG suites of the Rio Maria granite-greenstone terrane: Implications for the growth of the Archean crust of the Carajás Province, Brazil. *Precambrian Research*, **187**(1-2):201-221. https://doi.org/10.1016/j.precamres.2011.03.004

Althoff F.J., Barbey P., Boullier A.M. 2000. 2.8 and 3.0 Ga plutonism and deformation in the SE Amazonian craton: the Archean granitoids of Marajoara (Carajás Mineral province, Brazil). *Precambrian Research*, **104**(3-4):187-206. https://doi.org/10.1016/S0301-9268(00)00103-0

Arne D., House E., Pontual S., Huntington, J. 2016. Hyperspectral interpretation of selected drill cores from orogenic gold deposits in central Victoria, Australia, *Australian Journal of Earth Sciences*, **63**(8):1003-1025. https://doi.org/10.1080/08120099.2016.1223171

Bettencourt J.S., Juliani C., Xavier R.P., Monteiro L.V.S., Bastos Neto A.C., Klein E.L., Assis R.R., Leite Jr. W.B., Moreto C.P., Fernandes C.M.D., Pereira V.P. 2016. Metallogenetic systems associated with granitoid magmatism in the Amazonian Craton: An overview of the present level of understanding and exploration significance. *Journal of South American Earth Sciences*, **68**:22-49. https://doi.org/10.1016/j.jsames.2015.11.014

Bishop J.L., Lane M.D., Dyar M.D., Brown A.J. 2008. Reflectance and emission spectroscopy study of four groups of phyllosilicates: Smectites, kaolinite-serpentines, chlorites and micas. *Clay Minerals*, **43**(1):3554. https://doi.org/10.1180/claymin.2008.043.1.03

Clark R.N. 1999. Spectroscopy of Rocks and Minerals, and Principles of Spectroscopy. In: Rencz A.N. (Ed.). *Remote Sensing for the Earth Sciences: Manual of Remote Sensing*. 3 ed. v. 3. John Wiley & Sons, Inc.

Costa e Silva E., Silva A.M., Toledo C.L.B., Mol A.G., Otterman D.W., Souza S.R.C. 2012. Mineral Potential Mapping for Orogenic Gold Deposits in the Rio Maria Granite Greenstone Terrane, Southeastern Pará State, Brazil. *Economic Geology*, **107**(7):1387-1402. https://doi.org/10.2113/econgeo.107.7.1387

Craveiro G.S., Villas R.N.N., Xavier R.P. 2019. Mineral chemistry and geothermometry of alteration zones in the IOCG Cristalino deposit, Carajás Mineral Province, Brazil. *Journal of South American Earth Sciences*, **92**:481-505. https://doi.org/10.1016/j.jsames.2019.02.009

Dall'Agnol R., Oliveira M.A., Almeida J.A.C., Althoff F.J., Leite A.A.S., Oliveira D.C., Barros C.E.M. 2006. Archean and Paleoproterozoic granitoids of the Carajás metallogenetic province, eastern Amazonian craton. *Magmatism, Crustal Evolution and Metallogenesis of the Amazonian Craton Symposium*. PRONEX-UFPA/SBG-NO, Abstracts Volume and Field Trips Guide, Belém, Brazil, 150 p.

Dardenne M.A. & Schobbenhaus C. 2001. *Metalogênese do Brasil*. Brasília: CPRM/UnB, Editora UnB, 392 p.

Gilbert F., Pascal M.L., Pichavant M., 1998. Gold solubility and speciation in hydrothermal solutions: experimental study of the stability of hydrosulphide complex of gold (AuHS°) at 350 to 450°C and 500 bars. *Geochimica et Cosmochimica Acta*, **62**(17):2931-2947. https://doi.org/10.1016/S0016-7037(98)00209-9

Goldfarb R.J., Groves D.I., Gardoll S. 2001. Orogenic Gold and geologic time: a global synthesis. *Ore Geology Reviews*, **18**(1-2):1-75. https://doi.org/10.1016/S0169-1368(01)00016-6

Gregory M.J., Lang J.R., Gilbert S., Hoal K.O. 2013. Geometallurgy of the Pebble copper-gold-molybdenum deposit, Alaska: Implications for gold distribution and paragenesis. *Economic Geology*, **108**(3):463-482. https://doi.org/10.2113/econgeo.108.3.463

Groves D.I., Goldfarb R.J., Santosh M. 2016. The conjunction of factors that lead to formation of giant gold provinces and deposits in non-arc settings. *Geoscience Frontiers*, **7**(3):303-314. https://doi.org/10.1016/j.gsf.2015.07.001

Harraden C.L., Mcnulty B.A., Gregory M.J., Lang J.R. 2013. Shortwave Infrared Spectral Analysis of Hydrothermal Alteration Associated with the Pebble Porphyry Copper-Gold-Molybdenum Deposit, Iliamna, Alaska. *Economic Geology*, **108**(3):483-494. https://doi.org/10.2113/econgeo.108.3.483

Herrmann W., Blake M., Doyle M., Huston D., Kamprad J., Merry N., Pontual S. 2001. Short wavelength infrared (SWIR) spectral analysis of hydrothermal alteration zones associated with base metal sulfide deposits at Rosebery and Western Tharsis, Tasmania, and Highway Reward, Queensland. *Economic Geology*, **96**(5):939-955. https://doi.org/10.2113/gsecongeo.96.5.939

Huhn S.R.B. 1992. *Geologia, controle estrutural e gênese do depósito aurífero Babaçu, região de Rio Maria, sul do Pará*. Thesis (Master's degree). Brasília: Universidade de Brasília, 169 p.

Hunt G.R. 1977. Spectral signatures of particulate minerals in the visible and near infrared. *Geophysics*, **42**(3):501-513. https://doi.org/10.1190/1.1440721

Hunt G.R., Ashley R.P. 1979. Spectra of altered rocks in the visible and near infrared. *Economic Geology*, **74**(7):1613-1629. https://doi.org/10.2113/gsecongeo.74.7.1613

Hunt G.R., Salisbury J.W. 1970. Visible and near-infrared spectra of minerals and rocks: I Silicate minerals. *Modern Geology*, **1**:283-300.

Hunt G.R., Salisbury J.W. 1971. Visible and near-infrared spectra of minerals and rocks: II Carbonates. *Modern Geology*, **2**:23-30.

Leite A.A.S., Dall'Agnol R., Macambira M.J.B., Althoff F.J. 2004. Geologia e geocronologia dos granitóides arqueanos da região de Xinguara–PA e suas implicações na evolução do Terreno Granito-Greenstone de Rio Maria, Cráton Amazônico. *Revista Brasileira de Geociências*, **34**(4):447-458. https://doi.org/10.25249/0375-7536.2004344447458

Mauger A.J., Ehrig K., Kontonikas-Charos A., Ciobanu C.L., Cook N.J., Kamenetsky V.S. 2016. Alteration at the Olympic Dam IOCG–U deposit: insights into distal to proximal feldspar and phyllosilicate chemistry from infrared reflectance spectroscopy, *Australian Journal of Earth Sciences*, **63**(8):959-972. https://doi.org/10.1080/08120099.2016.1264474

McLeod R.L., Gabell A.R., Green A.A., Gardavsky V. 1987. Chlorite infrared spectral data as proximity indicators of volcanogenic massive sulphide mineralisation. *Pacific Rim Congress '87*, Gold Coast, Queensland, August 26–29, 1987. Proceedings, p. 321-324.

Melo G.H.C., Monteiro L.V.S., Xavier R.P., Moreto C.P.N., Arquaz R.M., Silva M.A.D. 2019. Evolution of the Igarapé Bahia Cu-Au deposit, Carajás Province (Brazil): Early syngenetic chalcopyrite overprinted by IOCG mineralization. *Ore Geology Reviews*, **111**:102993. https://doi.org/10.1016/j.oregeorev.2019.102993

Melo G.H.C., Monteiro L.V.S., Xavier R.P., Moreto C.P.N., Santiago E.S.B., Dufrane E.A., Aires B. 2017. Temporal Evolution of the giant Salobo IOCG deposit, Carajás Province (Brazil): constrains from paragenesis of hydrothermal alteration and U-Pb geochronology. *Mineralium Deposita*, **52**(5):709-732. https://doi.org/10.1007/s00126-016-0693-5

Naleto J.L.C., Perrotta M.M., Costa F.G., Souza Filho C.R. 2019. Point and imaging spectroscopy investigations on the Pedra Branca orogenic gold deposit, Troia Massif, Northeast Brazil: implications for mineral exploration in amphibolite metamorphic-grade terrains. *Ore Geology Review*, **107**:283-309. https://doi.org/10.1016/j.oregeorev.2019.02.019

Nguimatsia F.W.D., Bolarinwa A.T., Yongue R.F., Ndikumana J.D., Olajide-Kayode J.O., Olisa O.G., Abdu-Salam M.O., Kamga M.A., Djou E.S. 2017. Diversity of Gold Deposits, Geodynamics and Conditions of Formation: A Perspective View. *Open Journal of Geology*, **7**(11):1690-1709. https://doi.org/10.4236/ojg.2017.711113

Oliveira M.A., Dall'Agnol R., Althoff F.J., Leite A.A.S. 2009. Mesoarchean sanukitoid rocks of the Rio Maria granite-greenstone terrane, Amazonian craton, Brazil. *Journal of South American Earth Sciences*, **27**(2-3):146-160. https://doi.org/10.1016/j.jsames.2008.07.003

Rio Doce Geologia e Mineração-Distrito Amazônia (DOCEGEO). 1988. Revisão litoestratigráfica da província mineral de Carajás, Pará. *35° Congresso Brasileiro de Geologia*, Volume: Província Mineral de Carajás, 11-54. Belém: SBG.

Sabóia A.M., Polo H.J.O., Sousa C.S., Silva R.C.S. 2018. *Mapa geológica-geofísica da folha SB.22-Z-C-III Xinguara*. Projeto integração geológica-geofísica-metalogenética das sequencias de Greenstone Belts do Domínio Rio Maria, Estado do Pará. Belém: CPRM. Escala 1:100.000.

Sandeman H.A., Rafuse H., Copeland D. 2010. *The setting of orogenic auriferous quartz veins at the Golden Promise prospect, central Newfoundland, and observations on veining and wall-rock alteration*. St. John's: Newfoundland Department of Natural Resources, Geological Survey, 16 p.

Souza C.S. 1999. *Gênese e controle do depósito aurífero de Lagoa Seca, Greenstone Belt de Andorinhas, Rio Maria, PA*. Thesis (Master's degree). Brasília: Universidade de Brasília, 162 p.

Souza S.R.C. 2018. *Mineralizações auríferas no Greenstone Belt Andorinhas, província mineral de Carajás, sudeste do estado do Pará*. Thesis (Doctorate). Brasília: Universidade de Brasília, 179 p.

Souza S.R.C., Botelho N.F., Dantas E.L., Jiménez F.A.C., Reis, M.A., Viana C.S. 2020. Geochemistry and isotopic geology of the Lagoa Seca gold deposit in the Andorinhas greenstone-belt, Carajás Province, Brazil. *Journal of South American Earth Sciences*, **99**:102523. https://doi.org/10.1016/j.jsames.2020.102523

Souza S.R.C., Botelho N.F., Jiménez F.A.C., Dantas E.L., Reis, M.A., Viana C.S. 2021. Mineralization and hydrothermal alteration in the Mamão orogenic gold deposit, Andorinhas greenstone belt, Carajás Province, Brazil. *Journal of South American Earth Sciences*, **112**(Part 1):103548. https://doi.org/10.1016/j.jsames.2021.103548

Souza Z.S., Potrel H., Lafon J.M., Althoff F.J., Pimentel M.M., Dall'Agnol R., Oliveira C.G. 2001. Nd, Pb and Sr isotopes of the Identidade Belt, an Archaean greenstone belt of the Rio Maria region (Carajás Province, Brazil): Implications for the Archaean geodynamic evolution of the Amazonian Craton. *Precambrian Research*, **109**(3-4):293-315. https://doi.org/10.1016/S0301-9268(01)00164-4

Squire R.J., Herrmann W., Pape D., Chalmers D.I. 2007. Evolution of the Peak Hill high-sulfidation epithermal Au-Cu deposit, eastern Australia. *Mineralium Deposita*, **42**(5):489-503. https://doi.org/10.1007/s00126-006-0076-4

Tappert M., Rivard B., Giles D., Tappert R., Mauger A. 2011. Automated drill core logging using visible and near-infrared reflectance spectroscopy: A case study from the Olympic Dam IOCG deposit, South Australia: *Economic Geology*, **106**(2):289-296. https://doi.org/10.2113/econgeo.106.2.289

Tassinari C.C.G., Macambira M.J.B. 1999. Geochronological Provinces of the Amazonian Craton. *Episodes*, **22**(3):174-182. https://doi.org/10.18814/epiiugs/1999/v22i3/004

Tassinari C.C.G., Macambira M.J.B. 2004. A evolução tectônica do Craton Amazonico. In: Mantesso e Neto V., Bartorelli A., Carneiro C.D.R., Brito Neves B.B. (Eds.). *Geologia do Continente Sul Americano: Evolução da obra de Fernando Flávio Marques Almeida*. São Paulo: Beca. p. 471-486.

Thompson A.A.B., Hauff P.L., Robitaille A.J. 1999. Alteration mapping in exploration: Application of shortwave infrared (SWIR) spectroscopy. *SEG Newsletter*, (39):1-27. https://doi.org/10.5382/SEGnews.1999-39.fea

Travers S.J., Wilson C.J.L. 2015. Reflectance spectroscopy and alteration assemblages at the Leven Star gold deposit, Victoria, Australia. *Australian Journal of Earth Sciences*, **62**(7):873-882. https://doi.org/10.1080/08120099.2015.1114525

Tunussi C. 2012. *Integração de dados multifonte para caracterização das zonas de alteração hidrotermal associadas às mineralizações de ouro no greenstone belt andorinhas, província mineral de Carajás*. Thesis (Master's degree). Brasília: Universidade de Brasília, 144 p.

Vasquez L.V., Rosa-Costa L.R., Silva C.G., Ricci P.F., Barbosa J.O., Klein E.L., Lopes E.S., Macambira E.B., Chaves C.L., Carvalho J.M., Oliveira J.G., Anjos G.C., Silva H.R. 2008. Escala 1:1.000.000. In: Vasquez M.L., Rosa-Costa L.T. (Eds.). *Geologia e Recursos Minerais do Estado do Pará: Sistema de Informações Geográficas e SIG: texto explicativo dos mapas Geológico e Tectônico e de Recursos Minerais do Estado do Pará*. Belém: CPRM. p. 113-216.

Villas R.N.N., Santos M.D. 2001. Gold deposits of the Carajás Mineral Province: deposit types and metallogenesis. *Mineralium Deposita*, **36**:300-331. https://doi.org/10.1007/s001260100178

Wilson C.J.L., McKnight S.W., Dugdale A.L., Rawling T.J., Farrar A.D., McKenzie M.J., Melling W.D. 2009. Illite crystallinity and the b-spacing values of white micas and their implications for gold mineralisation in the Lachlan Orogen, *Australian Journal of Earth Sciences*, **56**(8):1143-1164. https://doi.org/10.1080/08120090903246238